Journal of Physics: Conference Series

PAPER • OPEN ACCESS

Multiscale Simulation of Offshore Wind Variability During Frontal Passage: Brief Implication on Turbines' Wakes and Load

To cite this article: Mostafa Bakhoday-Paskyabi *et al* 2022 *J. Phys.: Conf. Ser.* **2362** 012003

View the article online for updates and enhancements.

You may also like

- UK perspective research landscape for offshore renewable energy and its role in delivering Net Zero
Deborah Greaves, Siya Jin, Puiwah Wong et al.
- A Flexible, Multi-fidelity Levelised Cost of Energy Model for Floating Offshore Wind Turbines Multidisciplinary Design, Analysis and Optimisation Approaches
V Sykes, M Collu and A Coraddu
- Estimating the value of offshore wind along the United States' Eastern Coast
Andrew D Mills, Dev Millstein, Seongeun Jeong et al.

BREATH BIOPSY

Breath Biopsy® OMNI®

The most advanced, complete solution for global breath biomarker analysis

TRANSFORM YOUR RESEARCH WORKFLOW

Expert Study Design & Management

Robust Breath Collection

Reliable Sample Processing & Analysis

In-depth Data Analysis

Specialist Data Interpretation

This content was downloaded from IP address 129.177.169.228 on 10/02/2023 at 13:32

Multiscale Simulation of Offshore Wind Variability During Frontal Passage: Brief Implication on Turbines' Wakes and Load

Mostafa Bakhoday-Paskyabi, Maria Krutova, Hai Bui, and Xu Ning
Geophysical Institute, University of Bergen, and Bergen Offshore Wind Centre, Bergen, Norway

E-mail: Mostafa.Bakhoday-Paskyabi@uib.no

Abstract. Enhancing the performance of offshore wind park power production requires, to a large extent, a better understanding of the interactions of wind farms and individual wind turbines with the atmospheric boundary layer over a wide range of spatiotemporal scales. In this study, we use a multiscale atmospheric model chain coupled offline with the aeroelastic Fatigue, Aerodynamics, Structures, and Turbulence (FAST) code. The multiscale model contains two different components in which the nested mesoscale Weather and Research Forecast (WRF) model is coupled offline with the Parallelized Large-eddy Simulation Model (PALM). Such a multiscale framework enables to study in detail the turbine behaviour under various atmospheric forcing conditions, particularly during transient atmospheric events.

1. Introduction

Offshore wind is one of the key renewable energy resources today and for the years to come. Therefore, a better understanding of wind and its spatiotemporal variability further offshore plays a significant role in future technical and technological developments in offshore wind industries. In some applications, the wind in the boundary layer is described using simple representations, such as power-law or logarithmic profiles. However, these simplified wind profiles cannot always properly capture the vertical distributions of observed wind, particularly, during transient atmospheric events such as Low-Level Jets (LLJs)–during stably stratified conditions, and Open Cellular Convection (OCC)–during convectively unstable conditions. In such conditions, the wind characteristics, such as wind shear, wind veer, and turbulence intensity, depart significantly from those assumed under standard conditions [1, 2, 3]. Furthermore, these transient events modify the performance of wind power generation and structural loading by impacting the turbine wake meandering, evolution, and recovery rates. Therefore, increased knowledge of site-specific characteristics of events like OCCs, their formation mechanisms, and their strengths and impacts are critical to improving farm power generation, turbine performance, and offshore wind turbine load assessments [4].

Areas covered by a large number of wind park clusters experience a large variability of wind speed and farm/turbine power fluctuations during the passage of OCCs. These transient frontal episodes are common atmospheric processes in the North Sea [2]. OCCs are associated with cold air advection over the warmer ocean surface and are visible from the satellite images as honeycomb-like patterns of shallow convective clouds (with 1km-3km thickness) [6, 2]. The

Content from this work may be used under the terms of the Creative Commons Attribution 3.0 licence. Any further distribution of this work must maintain attribution to the author(s) and the title of the work, journal citation and DOI.
Published under licence by IOP Publishing Ltd

vertical velocity is positive in the updraft regions at the cloudy edges of cells and is negative in the downdraft regions at the cloud-free cell centres. Spatial scales of the cell in the Southern North Sea vary between 7km and 80km with a temporal scale of minutes to hours. The spatiotemporal behaviour of the OCCs at their multiple scales can be efficiently captured by the use of an appropriate atmospheric multiscale modelling system.

Over the last couple of years, numerical research of flow field modelling in the offshore wind energy applications has developed by coupling between the mesoscale Numerical Weather Prediction (NWP) models and microscale high fidelity Large Eddy Simulation (LES) models [1]. NWPs are primarily Reynolds-Averaged Navier–Stokes (RANS) models, in which the turbulence is parameterized based on averaged properties of the flow fields. However, LES models (for example the Parallelized Large-eddy Simulation Model, or PALM) resolve turbulent eddies larger than a spatial lengthscale (large eddies) and parameterize the eddies smaller than the spatial filter lengthscale (subgrid scales) [8, 9]. While LES models have been primarily used in idealised simulations, they can represent realistic flow evolution if the effects of time-varying mesoscale flows along their outermost boundaries are implemented properly through an (one-way) offline nesting approach [10]. PALM system is able to use the mesoscale data from the regional weather prediction model such as Consortium for Small-scale Modeling (COSMO) and the Weather Research and Forecast (WRF) [11] models. The PALM model also contains the implementation of a wind turbine actuator disk parameterization with rotation that enables the multiscale framework to predict more precisely the turbulent flow within the wind park under realistic atmospheric forcing conditions. However, these types of simulations are subjected to several uncertainties associated with the boundary forcing information, the land-use characteristics, the choice of roughness length, etc. [1].

In this work, we develop a multi-scale model chain consisting of the WRF and the PALM models: the WRF model downscales large-scale features and provides the lateral forcing for the PALM model to perform LES simulation using a grid nesting approach. This modelling system provides the LES model with a more realistic time-dependent inflow condition that enables it to capture the variability of a broad range of differently stratified flows. The primary objectives of this study are then:

- to tentatively assess the added value of simulations with the suggested multiscale framework.
- to preliminary study and improve the understanding of the effects of thermally-driven flows on wake evolution and the turbine load behaviour during an OCC event at the area of Alpha Ventus offshore wind park.

While the LES model can provide a non-Gaussian representation of inflow winds, to be used for the load study, we simplify our analysis by assuming that the inflow turbulence field is completely Gaussian by applying a so-called constrained turbulence generator that uses the LES high-frequency time series at a number of separated points.

In this paper, we first introduce the site and its environmental conditions. The methodology is then given in Section 3, and the multiscale model results and structural loading are presented in Section 4. Finally, some conclusions are given in the last section.

2. Observational data and case study

The 100-m tall FINO1 meteorological mast (with coordinates of $54^{o}0^{'}53.5^{"}$N, $6^{o}35^{'}15.5^{"}$E) is located in the Southern North Sea in a water depth of 30m, see Fig. 1. The mast is equipped with various sensors to measure different atmospheric quantities such as wind velocity at 33, 40, 50, 60, 70, 80, 90, and 100 m. High-frequency measurements were collected by sonic anemometers at 40, 60 and 80 m with a sampling frequency of 10 Hz, with an orientation of 308^{o} in order to remove the mast shadow zone during the data analysis step. During the NORCOWE OBLEX-F1 campaign between May 2015 and October 2016 at FINO1, two additional sonic anemometers

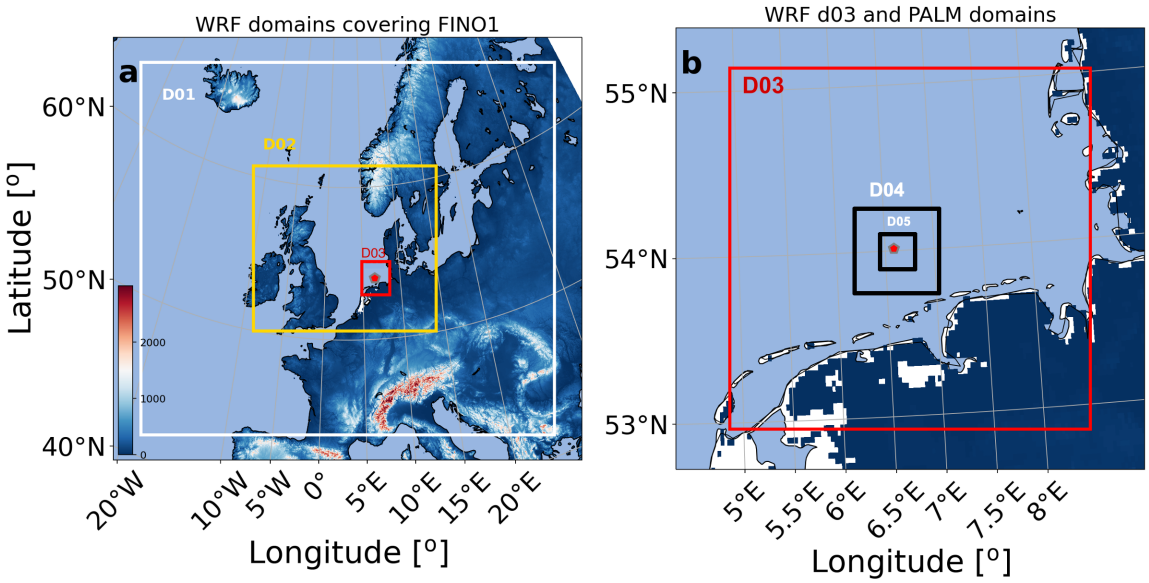

Figure 1. (a) The WRF's nested domains used in this paper with the horizontal resolutions of 9 km (D01), 3 km (D02), and 1 km (D03); and (b) the WRF's 1-km domain (D03) along with the PALM's two nested domains with horizontal resolutions of 375 m (D04) and 10 m (D05). The FINO1 platform is indicated by the red markers in both panels.

with a sampling frequency of 25Hz and an orientation angle of 135° were installed at 15m and 20m above the mean sea level. Waves were measured by a Datawell MKIII buoy deployed in close vicinity of the FINO1 mast.

The Alpha Ventus wind park operating in the vicinity of the FINO1 meteorological mast covers an area of 4km^2 and contains 12 wind turbines (M5000-116) with a hub height of 90 m and rotor top height of 148 m.

Figure 2-a shows a 10-min averaged time series of wind and wave characteristics at FINO1 and the vicinity for a 12-day period in November 2015, when there exhibits a range of variability and fluctuations in wind speed corresponding to several OCC events. The wind speed varies from 2 m/s to nearly 25 m/s with the wave height closely correlated with the wind (i.e. suggesting an almost fully developed sea). During the first period of OCC (between 02 UTC November 22 and 00 UTC November 23), the wave has the heights varying around 3 m and is primarily aligned with the wind (Fig. 2b). The OCC events are characterized by a warmer ocean surface than the overlying air (Fig. 2c). The second strong OCC event occurs between 06 UTC November 23 and 00 UTC November 24 when the wind and wave are even more aligned. Table 1 contains the characteristics of the averaged wind and wave during these two OCC events that occurred during the study period.

3. Methodology

3.1. WRF multiscale simulation setup

The Advanced Research WRF (ARW) version 4.3 is used for the mesoscale simulations of the OCC events and wind farm wakes for areas covering the offshore FINO1 meteorological mast. Figure 1-a represents the three-nested-domain setup of WRF. The outermost parent domain, D01, has a horizontal grid resolution of 9 km; the intermediate and innermost domains, D02 and D03, use 3-km and 1-km horizontal spacing, respectively. We use 60 vertical η-level with

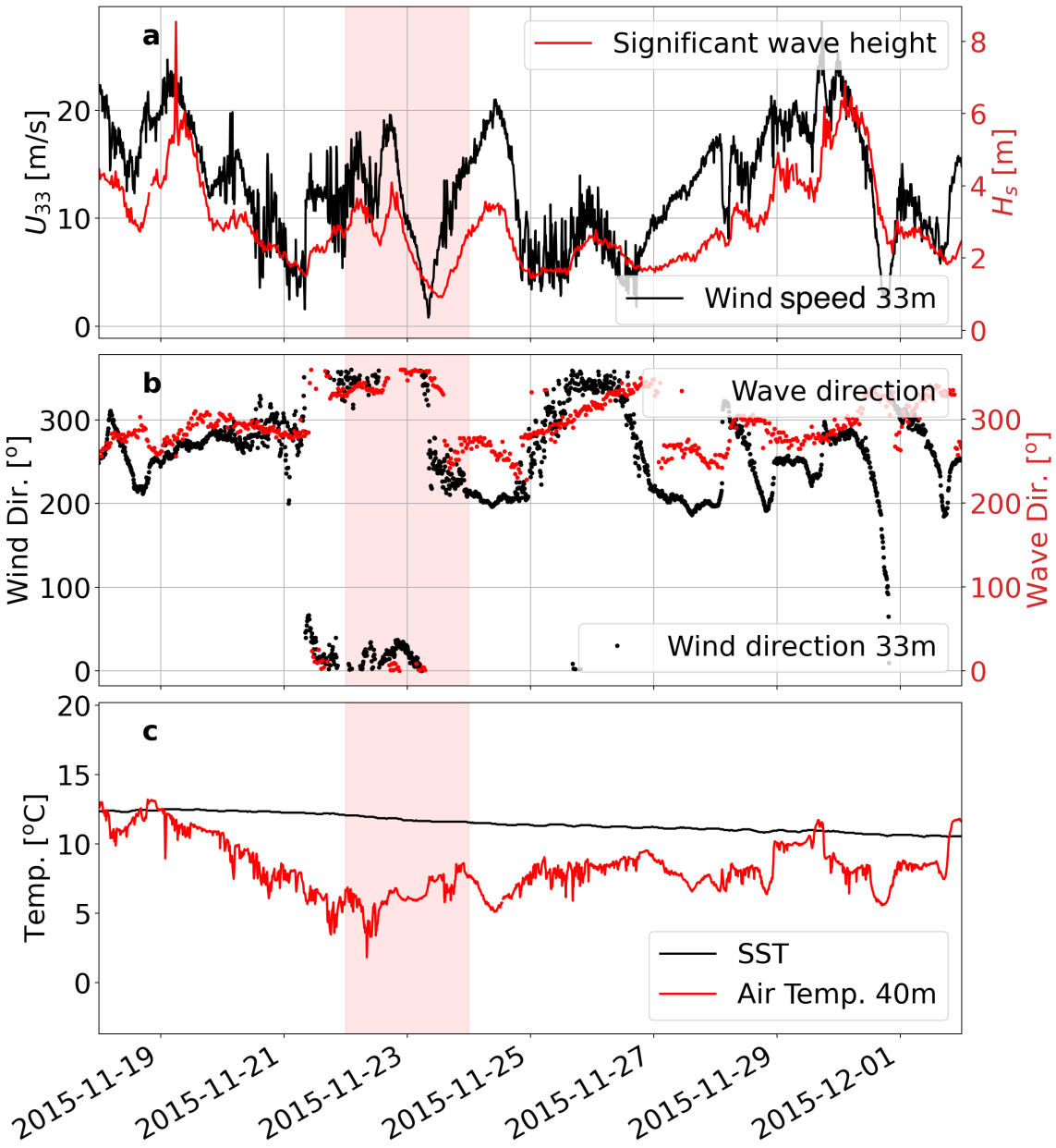

Figure 2. Time series during a 12-day period in November 2015 of (a) 33-wind speed measured by the 33-m height cup anemometer on the FINO1 met-mast (U_{33}, black line) and significant wave height measured by a moored buoy in the vicinity of FINO1 (H_s, red line); (b) wind direction at 33 m height measured by FINO1's wind vane (black dots) and wave direction (red dots); and (c) Sea Surface Temperature (SST) (black line) and air temperature at 40 m (red line). The red shaded area between November 22–24 highlights the WRF simulation period.

the highest vertical grid resolution near the surface for all three domains with 21 levels below 500 m (covering appropriately the measurement heights and the rotor plane area of turbines).

We initialized WRF with ERA5 reanalysis data and conducted a 2-day WRF simulation between November 22 and 24, 2015 (in which convective cells were generated and propagated over the FINO1 and Alpha Ventus wind park regions) using the contiguous US (CONUS) physics

Table 1. Summary of the averaged wind and wave data sets during two OCC events between November 22 and 24 2015. Here, T_p denotes the wave peak period, measured by the buoy nearby the FINO1 location.

Variables	U_{33} [m/s]	Wind direction [°]	H_s [m]	T_p [s]	Wave direction [°]
OCC1	14.3	251.0	3.2	8.4	337.0
OCC2	8.8	212.2	1.5	6.1	259.0

suite configuration. The physics suite contains the microphysics parameterisation developed by Thompson et al. (2008) [12], the Rapid Radiative Transfer Model and Dudhia schemes [13] for longwave and shortwave radiation calculations, the Tiedtke cumulus parameterisation, the eta similarity scheme for the surface layer parameterisation, and the unified Noah land surface model. We considered a spin-up time of 12 h and we did not apply the data assimilation technique in this study. We used the MYNN planetary boundary layer scheme to enable the use of the wind farm parameterization using the Fitch scheme [5]. Furthermore, we use the Met Office's Operational Sea-surface Temperature and Sea Ice Analysis (OSTIA) dataset due to the importance of the SST to study the OCC transient event. The daily OSTIA data are interpolated in time in order to match with hourly ERA5 input data.

3.2. PALM microscale simulation setup

We used the PALM model (version 21.10) to study the flow field variability in the area of the Alpha Ventus wind park and to provide (Gaussian) turbulent inflow boundary information for the wind turbine load study. PALM is an open-source LES code that models both the atmosphere and the ocean and is based on solving the non-hydrostatic incompressible Boussinesq approximation, along with the mass and energy conservation equations [8, 9]. Effects of turbines in the PALM are based on an Actuator Disk Model with Rotation (ADM-R). We used the ADM-R parameters to account for the NREL 5 MW reference turbine and to model the turbine/farm-affected flow fields in the area of Alpha Ventus wind park.

The PALM simulation domains are shown in Fig. 1-b. The parent domain covers the study site with a size of approximately 141 km (east-west)$\times$ 141 km (south-north). The grid sizes of this domain are $\Delta x = \Delta y = 275$ m and $\Delta z = 40$ m. The twelve wind turbines of the Alpha Ventus locates within the child domain with the grid sizes of $\Delta x = \Delta y = 11$ m and $\Delta z = 5m$.

3.3. Meso-to-microscale modeling system

With the offline nesting strategy, non-cyclic boundary conditions are applied to achieve a more realistic meteorological representations inside the PALM domain. Instead, the WRF outputs are used to create lateral and top boundary conditions for PALM, which include [10]: thermodynamics and velocity fields; vertical grid structure; soil information; and some geographical information. The boundary conditions for the PALM's outer domain are updated every 10 minutes, which is the WRF's output frequency. Since the WRF outputs do not contain turbulence, a synthetic turbulence generator is then used to generate the turbulence in time and space.

3.4. Structural analysis code

We conducted aeroelastic simulations based on the open-source software FASTv8 (developed by NREL) to model wind turbine responses during the frontal passage [7]. FAST contains embedded subroutines for the aerodynamic code that works based on the blade element momentum theory and the hydrodynamic module. Using a constraint turbulence generator (here TurbSim) and LES

time series (with a sampling frequency of 25 Hz) at vertical points located at FINO1 distributed over different heights from the near-surface (7.5 m) to below 250 m (so-called constraint points or pattern), we created the (Gaussian) inflow (3D turbulent wind fields) for the FAST program that computes then the time-series of blade momentums and forces. The FAST simulations are made on a 5-MW tripod-foundation wind turbine. The hydrodynamic loads (by HydroDyn FAST) on the supporting structure are modelled for the irregular waves (we use JONSWAP empirical spectrum to reconstruct the irregular waves based on wave bulk parameters measured during the study period).

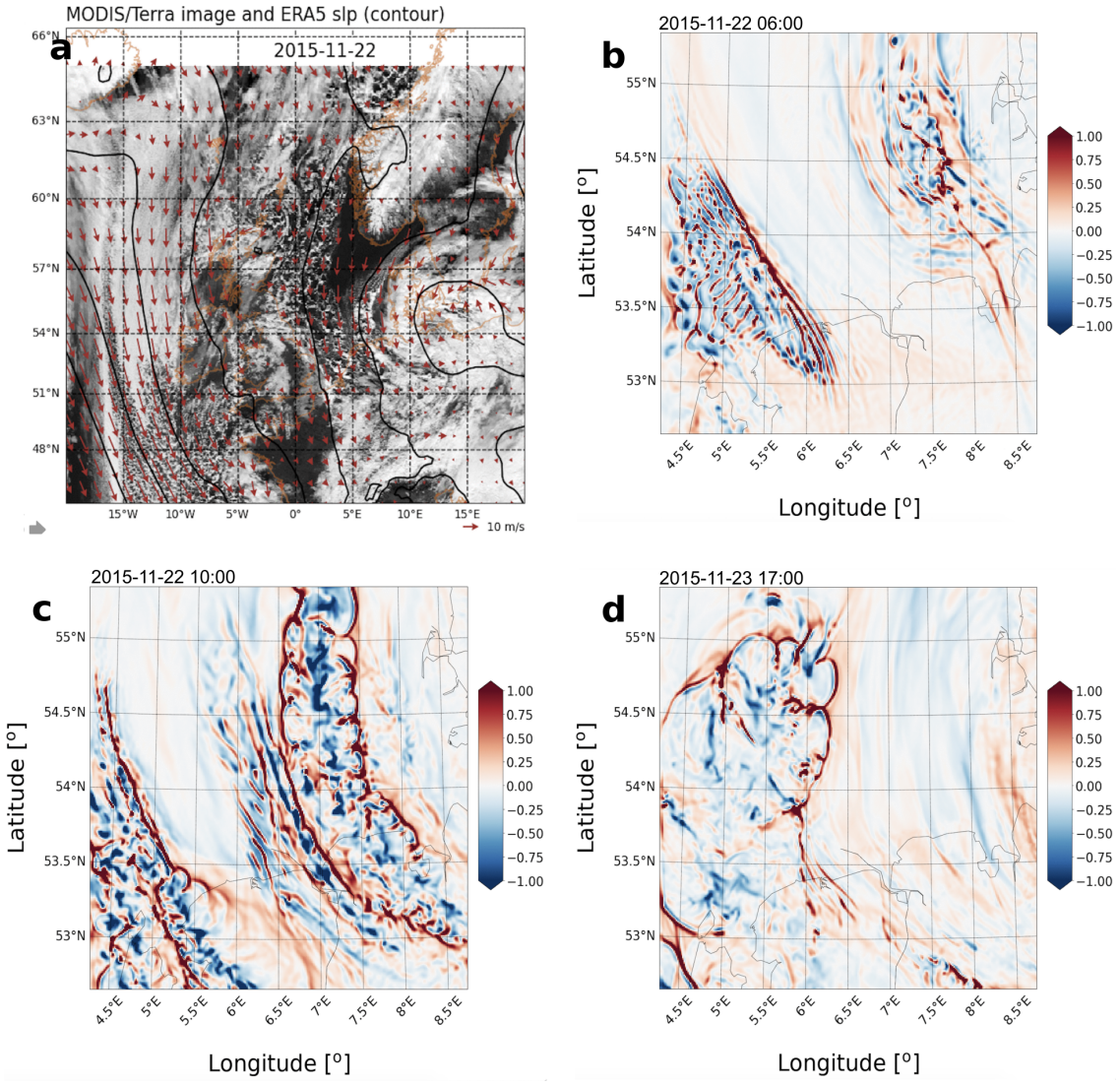

Figure 3. (a) The terra/MODIS satellite cloud image at 00 UTC November 22, 2015, from https://wvs.earthdata.nasa.gov; and the WRF vertical velocities at 100-m height at (b) 06 UTC November 22; (c) 10 UTC November 22; and (d) 17 UTC November 23 respectively.

The stochastic wind was generated by TurbSim on a 16×16 grid with $\sim$ 13-m width. The model uses time series of PALM at the constraint points and coherence parameters from model datasets as inputs. The PALM 25-Hz wind is aligned with the mean wind at each point in space

and the Davenport coherence in the TurbSim simulator, γ, is applied as follows:

$$\gamma(f) = \exp\left(-C\frac{f\delta}{\bar{u}}\right), \tag{1}$$

with the parameters estimated from the coherence in the PALM high-frequency wind data. Here, f denotes frequency, δ is the separation distance between the locations of two given time series, $\bar{u}$ is the mean wind speed, and C represents a decay coefficient (C can be computed separately for each velocity component). The surface roughness, power-law exponent for the wind profile, and wave parameters are found from the wind and wave measurements (see Table 1). In this paper, we used three load quantities calculated by FAST: the rotor speed F_t, the blade pitch, and blade 1 out-of-plane deflection.

4. Results

In this work, we study the OCC event that occurred on November 22, 2015, and Fig. 3-a shows the observed hexagonal cloud patterns of this event from the satellite image over the North Sea. This transient event was the result of a cold air outbreak when the cold and dry air behind an extratropical cyclone was advected from the north-northwest over a relatively warmer ocean surface (see Fig. 2-c). Figure 3-a provides a qualitative impression of the sizes, distributions, and locations of the convective cells over the North Sea and particularly over the study site. The OCC structures are revealed in the snapshots of vertical velocity at 100-m height from the WRF simulation at 1-km resolution (Fig. 3b-d). The wind parks operating in the Southern North Sea may experience substantial and harsh wind speed and wind direction differences during the passage of this front. In such convective conditions, both turbulence vertical/lateral mixing as well as the increase of unstable stratification, lead to narrow updraft edges (positive vertical velocity) and downdraft regions (negative vertical velocity at cell centres). Qualitative and visual comparisons between WRF model results and the satellite image suggest some general similarities in spatial distributions of cells over the North Sea. This event remains strong until approximately 20 UTC November 22, 2015 (Fig. 3-d).

Figures 4a-b show the WRF simulations of horizontal wind speed and vertical velocity extracted at the closest grid point to the FINO1 location (see Section 2 and Fig. 1). Short-timescale fluctuations are produced by WRF for both horizontal and vertical wind components under the OCC, and the patterns of convective circulation are observed clearly through the diverging downdrafts and the converging updrafts. The WRF simulation performed well when we compare the 100-m wind speed with the observation (Fig. 4c). Figure 4c also shows significant fluctuations during the passage of convective cells, where the WRF successfully captures the locations of cells and some of the variations.

For the LES simulation, we coupled WRF with the PALM model through a one-way, offline nesting approach. We first run the mesoscale simulation (i.e. WRF with domains D01–D03) for the entire study period and created the boundary file from the 1-km (D03) resolution results to force the flow fields inside the PALM parent domain (D04), which were then nested onto the innermost domain (D05) through PALM-PALM nesting scheme. We conducted two microscale experiments to simulate high-frequency time series of wind speed at different heights at the location of FINO1 met-mast: (1) before the first frontal passage (starting from 00UTC, November 22) for 20min); and (2) the onset of the first OCC event (starting from 02 UTC, November 22 for 20min). Within D05, we included 12 5-MW NREL wind turbines at geographical locations of Alpha Ventus turbines. Besides the general mean outputs, we included the 25-Hz high-frequency sampling outputs at points covering the rotor area of one turbine in the first row of Alpha Ventus farm to study the non-Gaussian turbulence later on, as well as vertically distributed points at the geographical location of FINO1 to be used in the Gaussian wind generator TurbSim. While the more thorough validation of WRF-PALM results

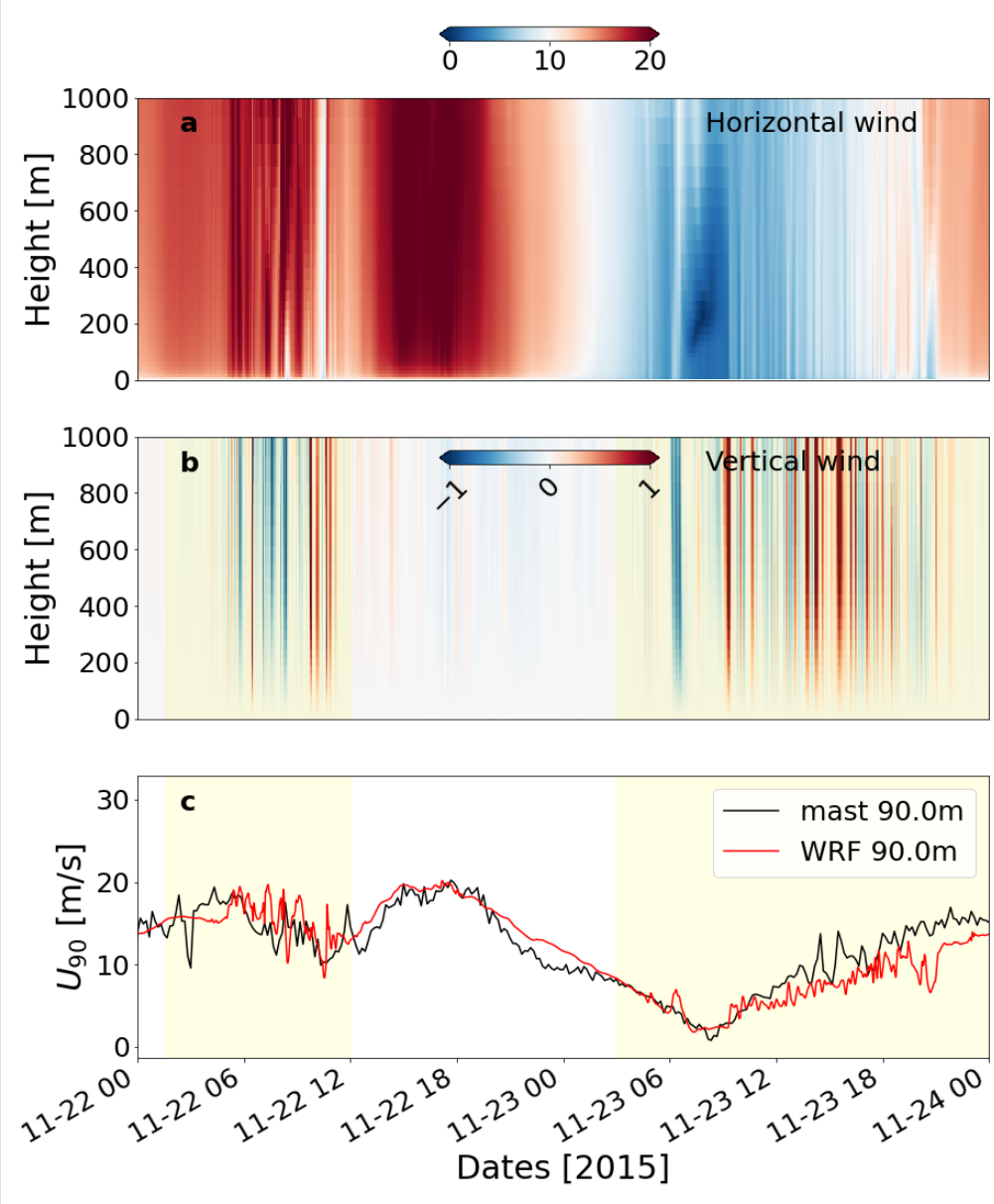

Figure 4. Time-height section at FINO1 over the study period November 22–24 2015 for (a) WRF's horizontal wind speed and (b) WRF's vertical velocity. Panel (c) compares the WRF's wind speed at 50-m height (red line) and measurements from FINO1's cup anemometer (black line). Shaded yellow areas in (b) and (c) show the periods of OCCs.

will be done in our next study, we illustrate the capability of our coupled WRF-PALM system to simulate the wind variability and the turbine wake before and during the OCC passage in Fig. 5. Before the frontal passage, the background flow is almost north-northeasterly which then rotates gradually to north-northwesterly as the front enters the farm region. It is observed that the yaw control of turbines may contribute to the wake meandering by turbines (we do not investigate how well the modelled yawing results match the observed SCADA data in this study).

To construct turbulence velocity fields as inflows of aeroelastic simulations, the necessary

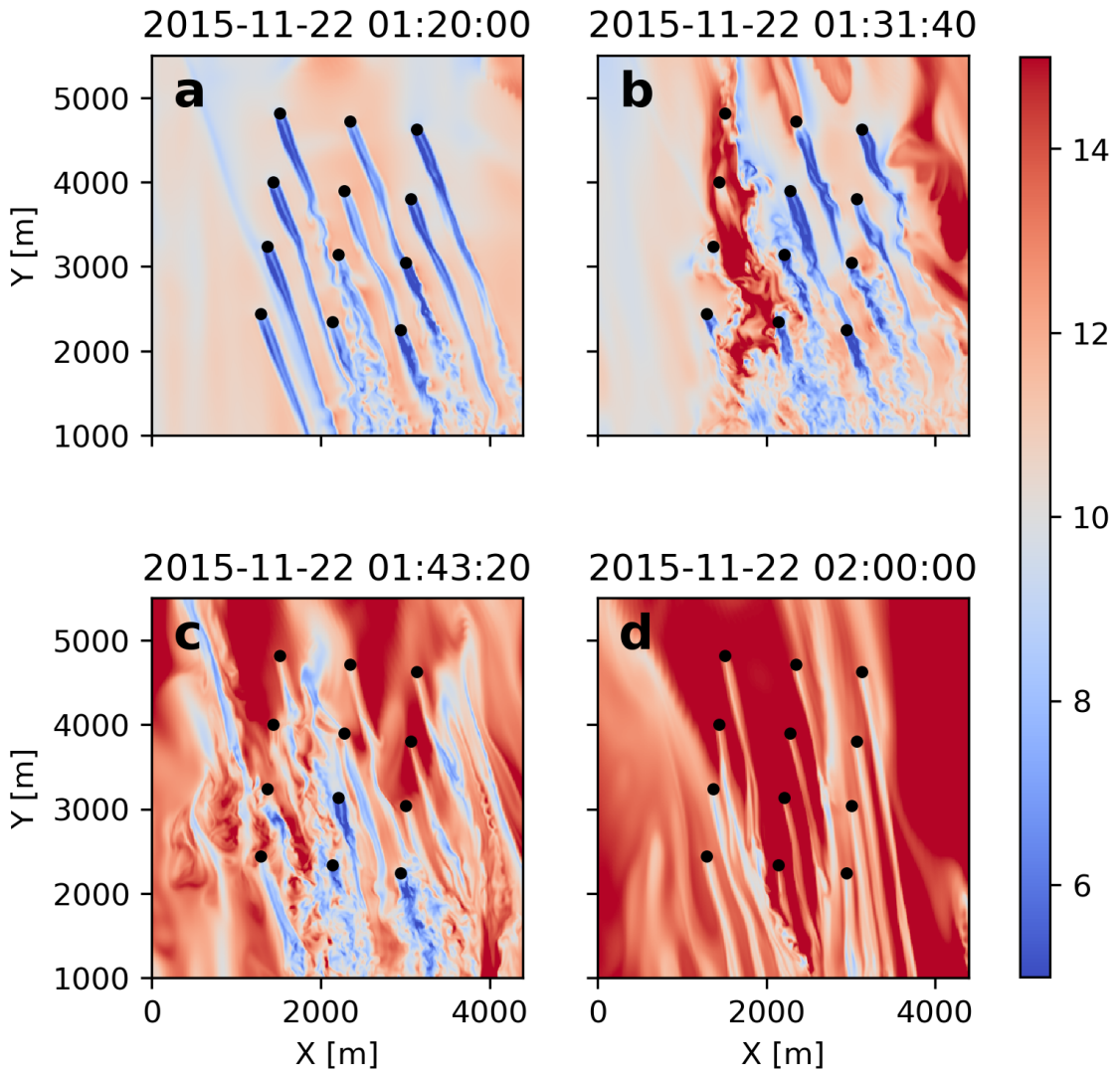

Figure 5. Hub-height wind speed comparison of PALM model results at child domain at the times: (a) before frontal passage; (b) close to the OCC event but still before its passage; (c) when OCC is entering the Alpha Ventus region; and (d) during the OCC event.

parameters of the simulator will be fitted to the measured time series at the given constraint spatial pattern. Figure 6 displays the power spectra of times series at two different heights (7.5 m in the left panels and 147.5 m in the right panels) to examine how large scale turbulent structures, as well as the inertial subrange, are extended before (hence. PREOCC) and during the OCC event. The enhanced variability in the wind energy is pronounced across almost all frequencies during open cells, particularly close to the sea surface.

Two sets of wind fields are generated for the PREOCC and OCC conditions. The 20min wind fields are fitted to the PALM time series at FINO1. Figure 7 shows the generated constraint wind fields by TurbSim simulator (hereafter TIMESER) for two cases. In the Davenport model of the TurbSim, we assumed equal decay parameters for horizontal and vertical separation distances. Note that the PALM generated wind fields may not be appropriately stationary and this will be explored and discussed in our future study.

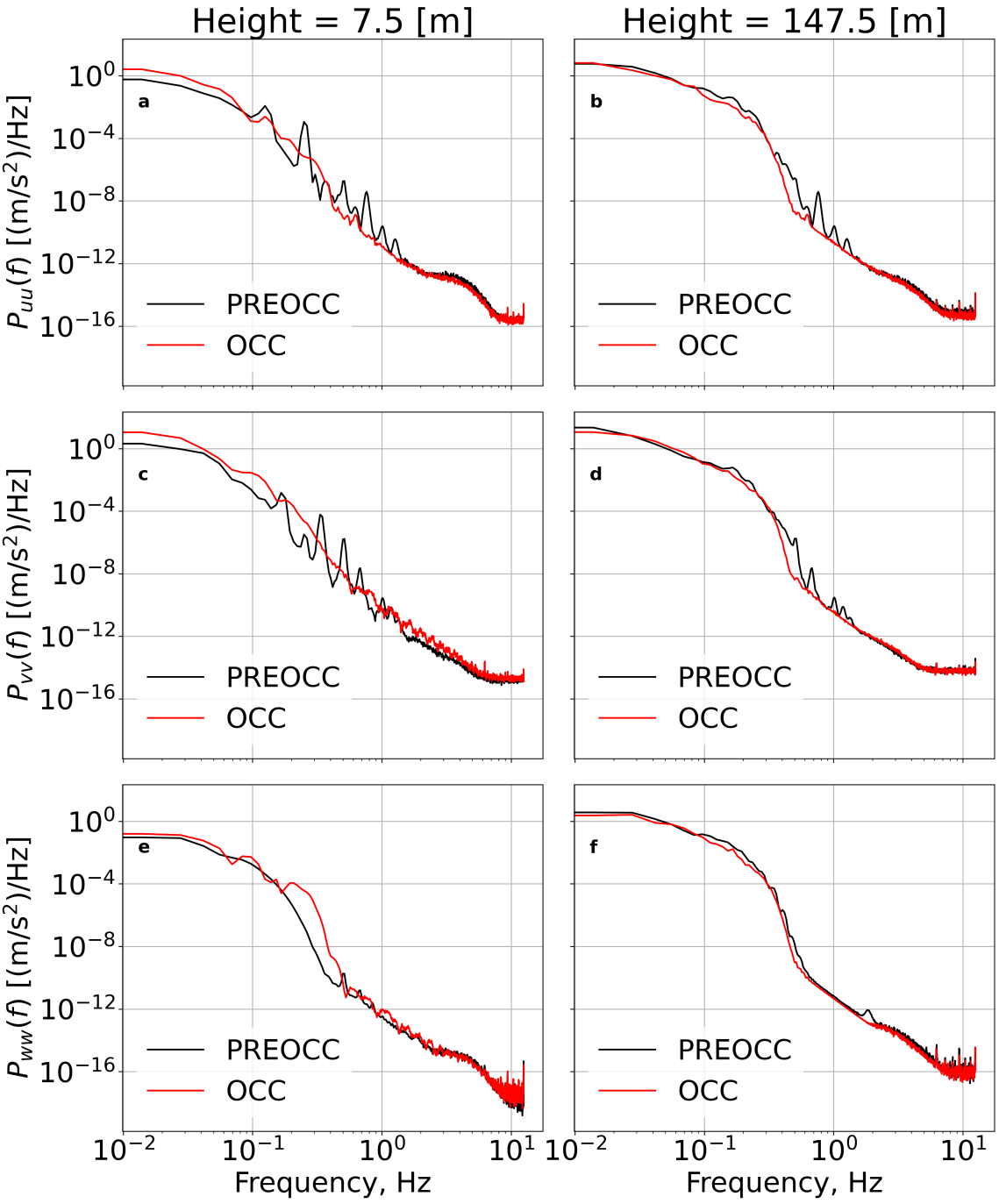

Figure 6. Comparisons of wind power spectra of PREOCC and OCC timeseries at FINO1 location at heights of 7.5m (a,c,e) and 147.5m (b,d,f) above the mean sea level. P_{uu}, P_{vv}, and P_{ww} denote the power spectra of horizontal and vertical wind components, respectively.

We calculate the aerodynamic loads by the use of wind inflows according to TIMESER for PREOCC and OCC conditions. A time step of 0.05 s and a total length of 600s are used in the FAST simulations. We drop the first 200s of simulations as the spin-up time of the model. Figure 8 shows the various response spectra of the following quantities: "OopDefl1" that represents the instantaneous out-of-plane tip deflections of blade 1 relative to the undeflected pitch axis;

"BldPitch1" that indicates the pitch angle of the first blade; and the "RotSpeed" that represents the rotor speed. In Fig. 8-a, the effect of OCC can be observed through its oscillatory behaviour on the out-of-plane blade tip deflection, the rotor speed, and the blade pitch angle (pitch angle during PREOCC is 0 degree and is not shown here). During the transient event, the variation of the wind inflows relative to the rotor induces oscillations in the rotor speed. The control system adjusts then the fluctuating power through the control of blade pitch angle (as shown in Fig. 8b, red line). PSDs in Fig. 8c show very different variations at low frequencies and PSDs in Fig. 8d show very similar behaviour with comparable energy levels at very low frequencies (and elevated energy levels at higher frequencies). The maximum OopDefl1 (of approximately 6m) occurs when wind speed drops and the pitch angle of the blade becomes 0^{o}.

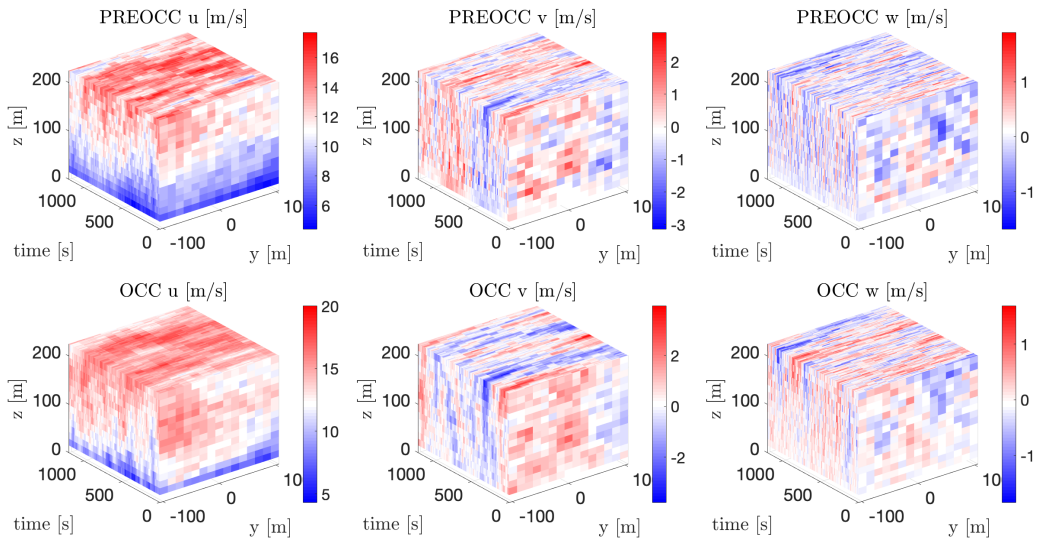

Figure 7. Three-dimensional turbulent wind boxes simulated by TurbSim constrained by 30 vertical points at FINO1 during: (a,b,c) OCC event; and (d,e,f) PREOCC event.

5. Conclusions

In this study, we presented a multi-scale modelling framework to simulate tentatively the propagation of the wind turbine wake as well as structural loads under a thermally-driven transient event (i.e. OCC). We utilized four model components in our model chain including: the WRF mesoscale model with three nested domains; the PALM microscale model with two nested domains combined with the actuator disk model with rotation; the TurbSim model generating the constraint turbulent wind fields; and finally the NREL FASTv8 structural code for investigating very briefly the structural responses of a 5-MW NREL wind turbine.

We implemented the offline nesting approach from the WRF to the PALM and conducted two experiments of WRF-PALM before the OCC (but very close to the onset of the OCC, PREOCC) and during the OCC event respectively. It was shown that the open convective cells modulate strongly the wake spatiotemporal evolution and load behaviour. Results preliminary showed the wake and load variations in the Alpha Ventus wind farm under OCC conditions and underlined the importance of using a multiscale framework to better understand the flow field and its variability, particularly during transient events in the offshore wind park regions.

We further explore the structural responses for the OCC event against another PREOCC event, in which the flow fields and environmental conditions are approximately similar to the

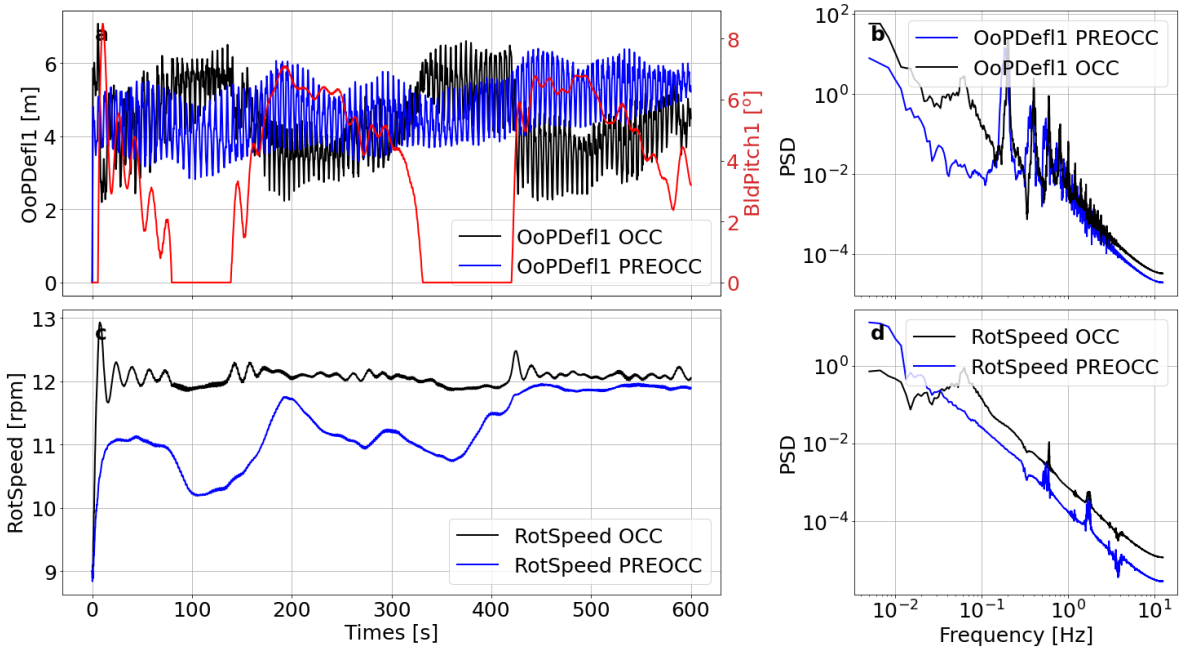

Figure 8. (a,c) Time series of turbine response from FASTv8 model; and (b,d) Power Density Spectra (PSDs) of out-of-plane tip deflections of blade 1 and rotor speeds before (PRECOCC) and during OCC event.

environmental conditions of the OCC.

We need, however, to conduct more comprehensive verification and validation procedures to assure the accuracy and performance of the presented coupled system. Furthermore, the selected PREOCC episode may have been affected by the OCC impacts. This necessitates further elaboration on the event selection.

Acknowledgments

The work is a part of the HIghly advanced Probabilistic design and Enhanced Reliability methods for high-value, cost-efficient offshore WIND (HIPERWIND) project, which has received funding from the European Union's Horizon 2020 Research and Innovation Programme under Grant Agreement No. 101006689. The simulations were performed on resources provided by UNINETT Sigma2 - the National Infrastructure for High Performance Computing and Data Storage in Norway. Some data used in this study are as part of the OBLEX-F1 field campaign that has been performed under the Norwegian Centre for Offshore Wind Energy (NORCOWE) funded by the Research Council of Norway (RCN 193821), the Offshore Boundary Layer Observatory (OBLO) project (project no. RCN 227777) and the Norwegian e-infrastructure NorStore (project no. RCN: NS9060K). OBLEX-F1 was coordinated in collaboration between the University of Bergen (Geophysical Institute) and NORCE Norwegian Research Centre (project executing organization). The Federal Maritime and Hydrographic Agency of Germany (BSH) is acknowledged for providing the FINO1 reference data through the FINO database at http://fino.bsh.de/. The FINO project is funded by the BMU, the German Federal Ministry for the Environment, Nature Conservation, Building and Nuclear Safety in collaboration with Project Management Jülich GmbH (project no. 0325321). The FINO1 meteorological reference data were provided by Deutsches Windenergi Institut (DEWI). We also thank the FINO1 platform operator Forschungs- und Entwicklungszentrum Fachhochschule Kiel GmbH (FuE Kiel

GmbH) for their support (project no. 0329905E).

References

[1] Arthur R S, Mirocha J D, Marjanovic N, Hirth B D, Schroeder J L, Wharton S, and Chow F K, 2020 Multi-Scale Simulation of Wind Farm Performance during a Frontal Passage, *Atmosphere*, **11**, 245, https://doi.org/10.3390/atmos11030245.

[2] Imberger M, Larsén X G, and Davis N, 2021 Investigation of Spatial and Temporal Wind-Speed Variability During Open Cellular Convection with the Model for Prediction Across Scales in Comparison with Measurements, *Boundary-Layer Meteorology*, 179:291–312, https://doi.org/10.1007/s10546-020-00591-0

[3] Bakhoday-Paskyabi M, Flügge M, 2021, Predictive Capability of WRF Cycling 3DVAR: LiDAR Assimilation at FINO1, *J. of Physics: Conference Series*, 1742–6596, http://dx.doi.org/10.1088/1742-6596/2018/1/012006.

[4] Krüger S, Steinfeld G, Kraft M, and Laura Lukassen L J, 2022 Validation of a coupled atmospheric–aeroelastic model system for wind turbine power and load calculations, *Wind Energ. Sci.*, **7**, 323–344, 2022

[5] Fitch A C, Olson J B, Lundquist J K, Dudhia J, Gupta A K, Michalakes J, and Barstad I, 2012, Local and mesoscale impacts of wind farms as parameterized in a mesoscale NWP model, *Mon. Weather Rev.*, **140**, 3017–3038.

[6] Göcmen T, Larśen X G, and Imberger M, 2020 The effects of Open Cellular Convection on Wind Farm Operation and Wakes, *J. Phys.: Conf. Ser.*, **1618**, 062014.

[7] Jonkman J M, Butterfield S, Musial W, and Scott G, 2009 Definition of a 5-MW reference wind turbine for offshore system development. Technical Report NREL/TP-500-38060, *National Renewable Energy Laboratory*, 1617 Cole Boulevard, Golden, Colorado 80401- 3393, February.

[8] Maronga B, Gryschka M, Heinze R, Hoffmann F, Kanani-Sühring F, Keck M, Ketelsen K, Letzel M O, Sühring M, and Raasch S, 2015 The Parallelized Large-Eddy Simulation Model (PALM) version 4.0 for atmospheric and oceanic flows: model formulation, recent developments, and future perspectives. *Geoscientific Model Development*, **8(8)**, 2515–2551.

[9] Maronga B, Banzhaf S, Burmeister C, Esch T, Forkel R, Fröhlich D, Fuka V, Gehrke K F, Geletič J, Giersch, S, Gronemeier T, Groß G, Heldens W, Hellsten A, Hoffmann F, Inagaki A, Kadasch E, Kanani-Sühring F, Ketelsen K, Khan B A, Knigge C, Knoop H, Krč P, Kurppa M, Maamari H, Matzarakis A, Mauder M, Pallasch M, Pavlik D, Pfafferott J, Resler J, Rissmann S, Russo E, Salim, M, Schrempf, M., Schwenkel J, Seckmeyer G, Schubert, S, Sühring M, von Tils R, Vollmer L, Ward S, Witha B, Wurps H, Zeidler J, and Raasch S, 2020 Overview of the PALM model system 6.0, *Geosci. Model Dev.*, **13**, 1335–1372, https://doi.org/10.5194/gmd-13-1335-2020.

[10] Lin D, Khan B, Katurj M, Bird L, Faria R, and Revell L E, 2021 WRF4PALM v1.0: a mesoscale dynamical driver for the microscale PALM model system 6.0, *Geosci. Model Dev.*, **14**, 2503–2524.

[11] Hellsten A, Ketelsen K, Sühring M, Auvinen M, Maronga B, Knigge C, Barmpas F, Tsegas G, Moussiopoulos N, and Raasch S 2021 A nested multi-scale system implemented in the large-eddy simulation model PALM model system 6.0, *Geosci. Model Dev.*, **14**, 3185–3214, https://doi.org/10.5194/gmd-14-3185-2021.

[12] Thompson G, Field P R, Rasmussen R M, and Hall W D, 2008 Explicit forecasts of winter precipitation using an improved bulk microphysics scheme: Part II: implementation of a new snow parameterization, *Mon Weather Rev* **136(12)**, 5095–5115, https://doi.org/10.1175/2008MWR2387.1.

[13] Dudhia J, 1989 Numerical study of convection observed during the winter monsoon experiment using a mesoscale two-dimensional model, *J. Atmos. Sci.*, **46**, 3077–3107.